



# Weakened Atlantic Meridional Overturning Circulation causes the historical North Atlantic Warming Hole



Kai-Yuan Li & Wei Liu

Most oceans over the globe have experienced surface warming during the past century, but the subpolar Atlantic is quite otherwise. The sea surface temperature cooling trend to the south of Greenland, known as the North Atlantic Warming Hole, has raised debate over whether it is driven by the slowing of the Atlantic Meridional Overturning Circulation. Here we use observations as a benchmark and climate models as a tool to demonstrate that only models simulating a weakened historical Atlantic overturning can broadly reproduce the observed cooling and freshening in the warming hole region. This, in turn, indicates that the realistic Atlantic overturning slowed between 1900 and 2005, at a rate of  $-1.01$  to  $-2.97$  Sv century $^{-1}$  ( $1\text{ Sv} = 10^6\text{ m}^3\text{ s}^{-1}$ ), according to a sea-surface-temperature-based fingerprint index estimate. Particularly, the Atlantic overturning slowdown causes an oceanic heat transport divergence across the subpolar North Atlantic, which, while partially offset by enhanced ocean heat uptake, results in cooling over the warming hole region.

The Atlantic Meridional Overturning Circulation (AMOC) is characteristic of the northward flow of warm salty water in the upper Atlantic and the southward return flow in the deep Atlantic<sup>1</sup>, serving as a major source for the northward Atlantic heat and salt transports and playing a vital role in global climate change<sup>2,3</sup>. The AMOC is suggested—albeit subject to debate<sup>4</sup>—to have been in a weakening trend since the last century based on paleo-proxy reconstructions<sup>5–7</sup>, and is projected to further slow during the twenty-first century<sup>8,9</sup>.

Amidst the historical AMOC slowdown, a long-term cooling trend of surface temperature has been observed to the south of Greenland<sup>10,11</sup> (Fig. 1a), which is known as the North Atlantic Warming Hole (NAWH)<sup>12</sup>, and in contrast to global warming elsewhere<sup>13</sup>. The formation of the NAWH was attributed primarily to the AMOC slowdown and associated meridional oceanic heat transport divergence across the North Atlantic<sup>2,12,14–16</sup>. This close AMOC-NAWH relationship was hence used for developing an AMOC index by ref. 5 or AMOC fingerprint by ref. 17. Particularly, the fingerprint of AMOC slowdown combines, in a dipole-like pattern, both sea surface temperature (SST) cooling in the NAWH and warming in the Gulf Stream region, which coincides with a northward shift of the Gulf Stream. Aside from the AMOC slowdown, the NAWH was argued to result from a variety of factors encompassing changes in the North Atlantic wind-driven gyre circulation<sup>18</sup>, North Atlantic storminess<sup>19</sup> and westerly winds<sup>20,21</sup>, and a more positive North Atlantic Oscillation<sup>22</sup>. Nevertheless, none of these mechanisms appears to be able to refute the role of the AMOC in light of the intrinsic link between North Atlantic thermohaline and wind-driven

circulations via the Gulf Stream<sup>23–25</sup> and the tight ocean-atmosphere coupling over the North Atlantic<sup>1,26–28</sup>.

The debate over the AMOC mechanism on the NAWH may stem from AMOC uncertainties in either observations or model simulations. Although direct AMOC observations from the RAPID array at 26.5°N in the North Atlantic show that the strength of the AMOC quantitatively relates to meridional heat and freshwater transports<sup>29–31</sup> and potentially influence the eastern subpolar gyre of the North Atlantic<sup>32</sup>, they have only been available for the last two decades<sup>33</sup>, whereupon the observed overturning change is likely influenced by AMOC multi-decadal variability<sup>34</sup> and cannot fully represent a long-term, centennial trend. On the other hand, a majority of climate models were reported to simulate a weakened historical AMOC from the fifth phase of the Coupled Model Intercomparison Project (CMIP5)<sup>35</sup>, but a strengthened AMOC during the twentieth century from the sixth phase (CMIP6)<sup>36</sup>. Such distinct historical AMOC changes between two-generation climate models are owing largely to different AMOC responses to anthropogenic aerosol forcing and aerosol-cloud interactions in models<sup>37</sup>, which involve diverse responses of the net surface shortwave radiation and atmospheric circulation over the North Atlantic and subsequent AMOC-related feedback<sup>38</sup>.

Indeed, from another perspective, the contrasting historical AMOC trends amongst CMIP5/6 models<sup>39</sup>, combined with centennial SST observations, enable us in this study to elucidate the AMOC mechanism on the NAWH while also justifying historical AMOC changes inferred from climate model simulations. The underlying rationale is to juxtapose the

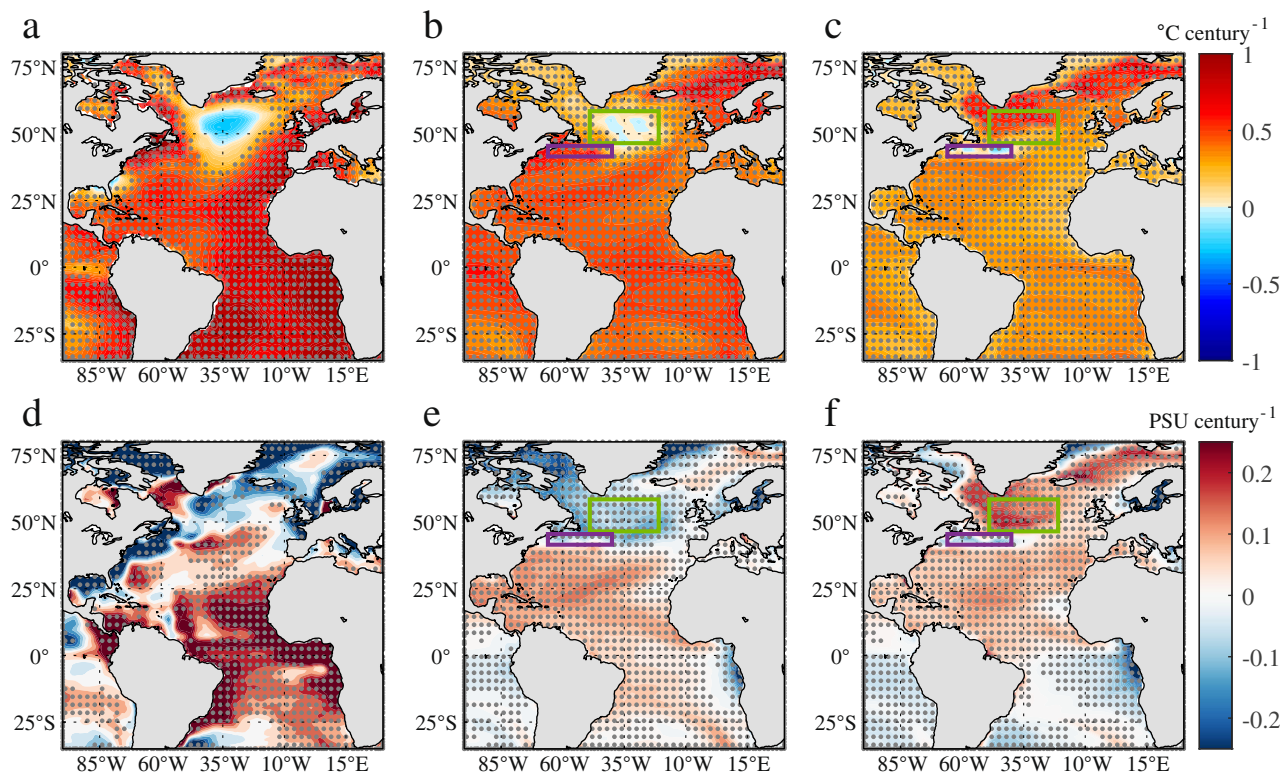


**Fig. 1 | Atlantic SST and SSS trends in observations and CMIP5/6 models.**

**a** Atlantic SST trend over 1900–2005 (color shading in  $^{\circ}\text{C century}^{-1}$ ) for the average of six observation datasets (COBEStv1 and v2, ERSSTv5 and v6, HadISST, and Kaplan Extended SSTv2). **b**, **c** Atlantic SST trends over 1900–2005 (color shading in  $^{\circ}\text{C century}^{-1}$ ) in historical simulations for the MMMs of **b** 51 AMOC- and **c** 43 AMOC+ models, respectively. **d** Atlantic SSS trend over 1955–2005 (color shading in  $\text{psu century}^{-1}$ ) for the average of three observation datasets (EN4, IAP, and Ishii).

**e**, **f** As in **b**, **c** but for the SSS trends over 1900–2005 (color shading in  $\text{psu century}^{-1}$ ). The stiples refer to the regions where trends are statistically significant based on Student's t-test at 95% confidence level. The green (subpolar gyre region; 46–58°N, 49–21°W) and purple (near Gulf Stream region; 41–45°N, 66–40°W) boxes in **b**, **c** and **e**, **f** are used for FPI calculation. Model drift from the pre-industrial control run has been removed from the model result.

simulated and observed SST trends to elicit whether a weakened or strengthened AMOC allows models to reproduce the observed NAWH cooling. Besides this AMOC-SST relationship, we will offer several lines of evidence leveraging long-term observations of sea surface salinity (SSS) and subsurface temperature and salinity to demonstrate the central role of the AMOC in the NAWH formation during the past century.

## Results

### AMOC and subpolar North Atlantic SST changes

We first examine the SST trend in six observational datasets (see “Methods”) from 1900 to 2005, as this centennial timescale minimizes the influence from decadal climate variability and the influence due to lags between AMOC strength and NAWH surface temperature and salinity changes within a decadal timescale<sup>32</sup>. We discover that, despite slight differences in location and strength, the NAWH is evident in all the datasets (Supplementary Fig. 1). The average of six observations exhibit a conspicuous cooling trend of annual mean SST up to  $-0.3\text{ }^{\circ}\text{C century}^{-1}$  to the south of Greenland, in contrast to the general SST warming in the rest of the Atlantic (Fig. 1a).

To compare model and observation, we exploit historical simulations with 41 CMIP5 models and 53 CMIP6 models (see “Methods”) and look into each model’s ensemble mean to reduce the impact of internal climate variability. We find that the majority of CMIP5 models (29 out of 41) simulate AMOC weakening trends between 1900 and 2005, whereas the majority of CMIP6 models (31 out of 53) simulate AMOC strengthening trends during the same period (Supplementary Table 1), which aligns well with previous research<sup>36</sup>. Nonetheless, there are substantial models from either CMIP phase that simulate historical AMOCs in the opposite trend as the major ones. We thus divide the 94 CMIP5/6 models into two categories:

weakened AMOC (51 models, referred to as AMOC- thereafter) and strengthened AMOC (43 models, referred to as AMOC+ thereafter). From 1900 to 2005, the AMOC trends for AMOC- and AMOC+ multi-model means (MMMs) are  $-1.35\text{ Sv}$  and  $1.24\text{ Sv century}^{-1}$  ( $1\text{ Sv} = 10^6\text{ m}^3\text{ s}^{-1}$ ), respectively. The annual mean SST trend for AMOC- MMM depicts a pattern similar to the observed NAWH, featuring an SST warming minimum or even cooling trend of up to  $-0.05\text{ }^{\circ}\text{C century}^{-1}$  south of Greenland away from stronger warming in the rest of the Atlantic (Fig. 1b). The AMOC- NAWH cooling may appear statistically insignificant and weaker for the MMM than the observed, likely related to different NAWH locations across models or between model and observation (see “Methods”); yet the cooling is statistically significant in certain individual models, with amplitude akin to observations<sup>40</sup>. In stark contrast, the AMOC+ MMM emphasizes an enhanced annual mean SST warming, rather than cooling, trend amounting to  $0.65\text{ }^{\circ}\text{C century}^{-1}$  to the south of Greenland (Fig. 1c). This result reveals that only models simulating a weakened AMOC can generally reproduce the observed NAWH cooling in the real world between 1900 and 2005.

### SST- and SSS-based AMOC fingerprint indices

We also notice a distinct dipole pattern of SST trend in either observation or model simulation, with annual mean SST cooling and warming in the subpolar North Atlantic and in the vicinity of the Gulf Stream region for observation and AMOC-, but opposite SST changes in both regions for AMOC+. Such distinct SST dipole manifests the AMOC fingerprint<sup>17</sup>, suggesting a decelerated AMOC in observation and AMOC- but an accelerated AMOC in AMOC+. Similar to the index by ref. 17, we define an SST-based AMOC fingerprint index ( $\text{FPI}_{\text{SST}}$ ) as the annual mean SST difference between the subpolar gyre and near Gulf Stream

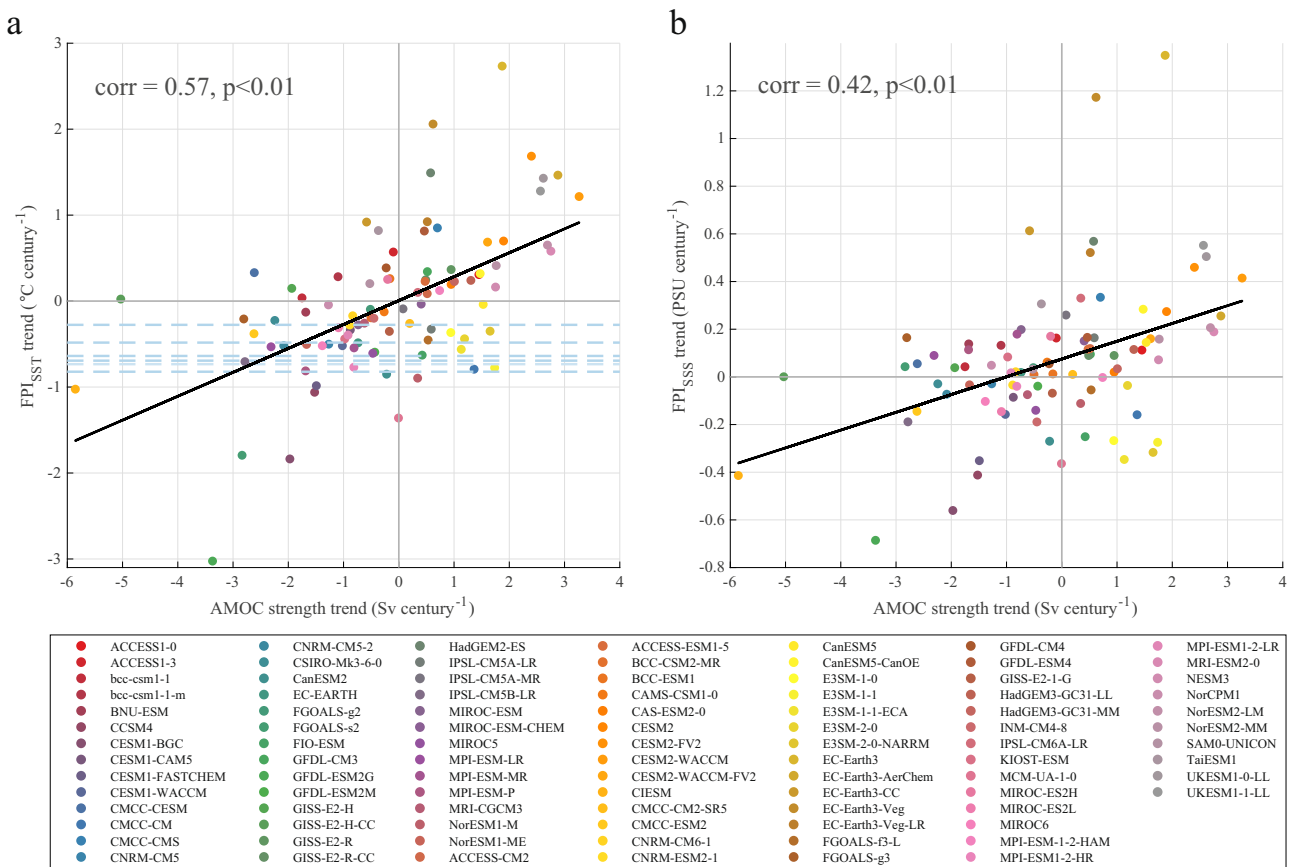


**Fig. 2 | Relationship between AMOC and FPI trends in CMIP5/6 models.** **a**, Scatter plot of AMOC strength and  $FPI_{SST}$  trends over 1900–2005 amongst 94 CMIP5/6 models (colored scatters). The correlation between the two trends is 0.57, statistically significant at the 95% confidence level, with corresponding regression line in black solid. Blue dashed lines denote the  $FPI_{SST}$  trends from six SST observations over 1900–2005. AMOC strength trends estimated from the regression line and the  $FPI_{SST}$

trends in COBESSTv1 and v2, ERSSTv5 and v6, HadISST, and Kaplan Extended SSTv2 are  $-1.01, -1.76, -2.66, -2.31, -2.97, -2.51$   $Sv\ century^{-1}$ , respectively. **b** As in **a** but for AMOC strength and  $FPI_{SST}$  trends over 1900–2005, whose correlation is 0.42, also statistically significant at the 95% confidence level. Model drift from the pre-industrial control run has been removed from the model result.

regions (see “Methods”). Combining all 94 CMIP5/6 models, we find a strong and significant correlation ( $0.57, p < 0.01$ ) between AMOC strength and  $FPI_{SST}$  trends over 1900–2005 (Fig. 2). Compared to ref. 17, we are able to sample both AMOC strength and  $FPI_{SST}$  trends over a broader range, with the former typically ranging from  $-3$  to  $3$   $Sv\ century^{-1}$  and the latter from  $-1$  to  $1$   $^{\circ}C\ century^{-1}$ . This means that the tight relationship between the overturning change and NAWH SST trend holds true for not only decelerated but also accelerated AMOC. Based on this relationship, the six SST observations provide an estimate of the realistic AMOC decline trend between  $-1.01$  and  $-2.97$   $Sv\ century^{-1}$  during 1900–2005. It should be noted that the correlation between AMOC strength and  $FPI_{SST}$  trends is also strong and significant when CMIP5 ( $0.42, p < 0.01$ , Supplementary Fig. 2a) and CMIP6 ( $0.54, p < 0.01$ , Supplementary Fig. 2c) models are considered separately.

We can infer the AMOC slowdown not only from SST trends but also from those in SSS. We investigate the annual mean SSS trend from 1900 to 2005 for CMIP 5/6 models and from 1955 to 2005 for observations. We choose 1955–2005 for the latter because it is the period during which all three salinity datasets are available (see “Methods”). The average of three observations (Supplementary Fig. 3) shows a significant freshening trend of annual mean SSS up to  $-0.25$   $psu\ century^{-1}$  across the NAWH (Fig. 1d). This long-term SSS decrease is supported by recently underwent freshening events over this region<sup>41,42</sup> and contrasts sharply with the salinity increase to the south (Fig. 1d). The AMOC- MMM experiences a pronounced SSS freshening over the NAWH (Fig. 1e) as consistent with observations. However, its freshening appears to extend to the Labrador Sea, where

observations point to an increase in SSS. This discrepancy may be attributed to the shorter SSS observation period, which allows for effects from multi-decadal climate variability. The AMOC+ MMM, on the other hand, displays an increasing trend in SSS over the NAWH but a decreasing trend in the vicinity of the Gulf Stream region, thereupon at odds with observations (Fig. 1f). Over the South Atlantic, both observation and AMOC- MMM witness a salinity buildup (Fig. 1d, e) due potentially to an AMOC slowdown<sup>43</sup>, whilst the AMOC+ MMM presents an SSS decrease there (Fig. 1f). These results evince that only models simulating a decelerated AMOC can generally replicate the observed NAWH freshening and South Atlantic salinity pile-up<sup>43</sup>; as such, the realistic AMOC has slowed between 1900 and 2005.

In line with  $FPI_{SST}$ , we define an SSS-based AMOC fingerprint index ( $FPI_{SSS}$ ) as the annual mean SSS difference between the subpolar gyre and near Gulf Stream regions (see “Methods”). Amongst all 94 CMIP5/6 models, a strong and significant correlation ( $0.42, p < 0.01$ ) emerges between AMOC strength and  $FPI_{SSS}$  trends over 1900–2005 (Fig. 2). This relationship is not specific to any one generation of the models, as the correlation is also strong and significant when CMIP5 ( $0.35, p < 0.05$ , Supplementary Fig. 2b) and CMIP6 ( $0.38, p < 0.01$ , Supplementary Fig. 2d) models are examined separately. Both  $FPI_{SST}$  and  $FPI_{SSS}$  indicate coherent SST and SSS changes over the NAWH, with surface cooling and freshening trends corresponding to an AMOC deceleration but opposite trends to an AMOC acceleration.

Moreover, NAWH cooling and freshening are not limited to the surface but extend into the subsurface ocean. Previous research found that the

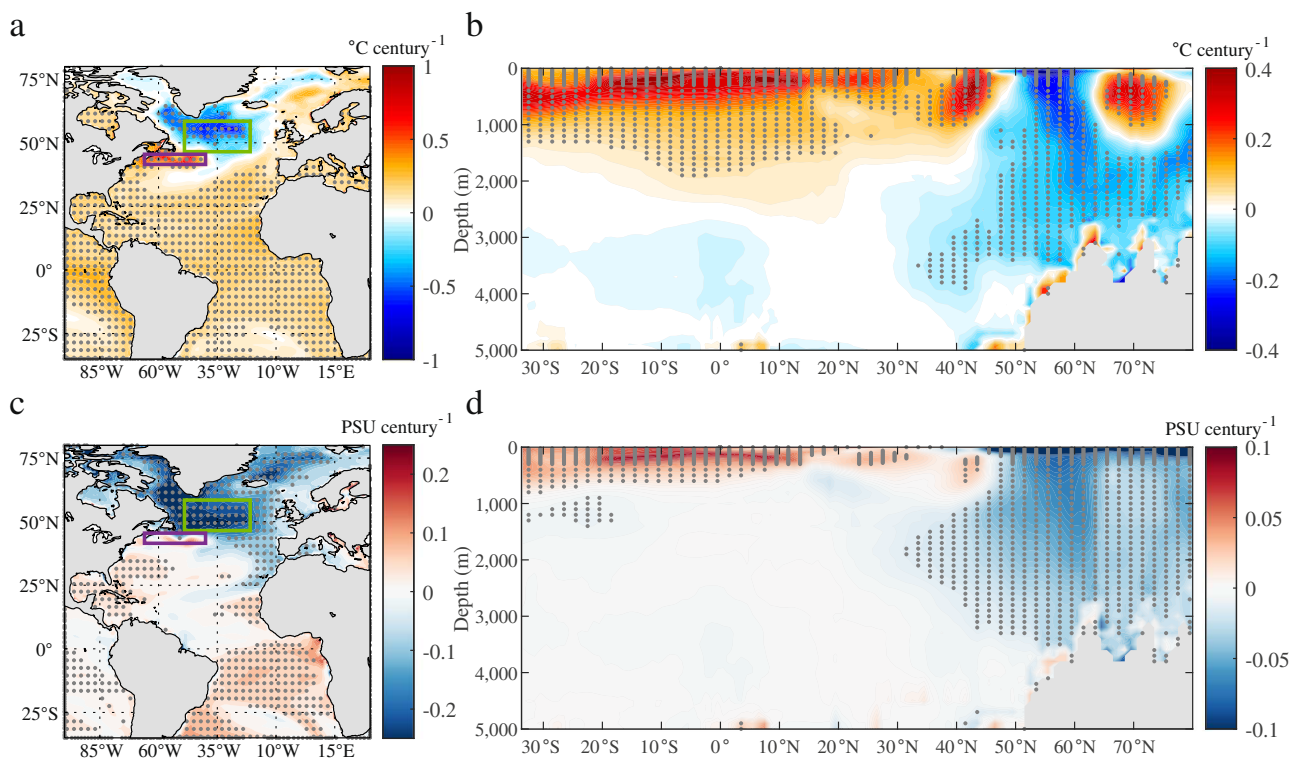


**Fig. 3 | Atlantic temperature and salinity trend differences between AMOC- and AMOC+.** Differences of Atlantic (a) SST and b zonal-mean ocean temperature trends over 1900–2005 (color shading in  $^{\circ}\text{C century}^{-1}$ ) based on historical simulations between the MMMs of 51 AMOC- and 43 AMOC+ models (AMOC- minus AMOC+). The stippling refer to the regions where differences are statistically

significant based on Student's t-test at 95% confidence level. c, d As in a, b but for SSS and zonal-mean salinity trends over 1900–2005 (color shading in  $\text{PSU century}^{-1}$ ). The green (subpolar gyre region;  $46\text{--}58^{\circ}\text{N}$ ,  $49\text{--}21^{\circ}\text{W}$ ) and purple (near Gulf Stream region;  $41\text{--}45^{\circ}\text{N}$ ,  $66\text{--}40^{\circ}\text{W}$ ) boxes in a, c are used for FPI calculation. Model drift from the pre-industrial control run has been removed from the model result.

CMIP5 MMM exhibits ocean cooling down to 1000 m over the NAWH region while warming beneath<sup>16</sup>. These vertical temperature changes could be the result of a combination of cooling caused by AMOC slowdown and background anthropogenic warming<sup>2</sup>. To eliminate the impact of background anthropogenic warming, we calculate the difference between AMOC- and AMOC+ MMMs in the zonal-mean temperature and salinity trends over the Atlantic during 1990–2005 (Fig. 3). Compared to a strengthened AMOC, the weakened AMOC creates cooling and freshening to the south of Greenland that contributes to the NAWH (Fig. 3a, c) and extends down to ocean bottom (Fig. 3b, d), which agrees with ref. 2. The composite analyses on CMIP5 and CMIP6 models, respectively, also show consistent results (Supplementary Figs. 4 and 5).

### Physical mechanisms

We further elucidate the role of AMOC slowdown in the NAWH formation by means of Atlantic Ocean heat budget that depicts a balance between ocean heat uptake, meridional gradient of oceanic heat transport (OHT), and ocean heat storage (see “Methods”). We leverage 9 AMOC- and 17 AMOC+ models that have all of the variables required for the heat budget calculation (Supplementary Table 1) and compute the difference of Atlantic Ocean heat budgets between AMOC- and AMOC+ MMMs from 1900 to 2005 (see “Methods”). Compared to a strengthened AMOC, the weakened AMOC produces a diminished northward OHT and hence a meridional OHT divergence in the North Atlantic, especially over  $40\text{--}65^{\circ}\text{N}$  (Fig. 4a). This OHT divergence serves as the primary cause of ocean cooling between  $40^{\circ}\text{N}$  and  $65^{\circ}\text{N}$  (Fig. 4b), seeing that the atmosphere acts to warm rather than cool the ocean in this region (Fig. 4a). The working mechanism for the atmospheric warming is the negative turbulent heat flux feedback<sup>44,45</sup>, via which the SST cooling in the subpolar North Atlantic can promote ocean heat uptake. In short, the AMOC slowdown brings about a meridional OHT divergence in the subpolar North Atlantic, which is partially offset by

increased heat uptake and results in cooling in the full-depth water column, manifesting as surface cooling over the NAWH.

Likewise, we leverage 2 AMOC- and 5 AMOC+ models that have all of the variables required for Atlantic salt budget calculation (Supplementary Table 1) and compute the salt budget difference between AMOC- and AMOC+ MMMs from 1900 to 2005 (see “Methods”). In response to AMOC slowdown, a meridional ocean salt transport divergence and the net positive, downward surface freshwater flux (equivalent to negative virtual salt flux) contribute almost equally to the freshening in the full-depth water column between  $45^{\circ}\text{N}$  and  $60^{\circ}\text{N}$  (Fig. 4c, d). Note that the salt-advection feedback<sup>46–48</sup> is still in effect; however, the different AMOC and surface freshwater flux responses to external anthropogenic forcings between AMOC- and AMOC+ serve as a major factor to the salt budget difference. Meanwhile, another feedback connecting NAWH SSS and SST and involving ocean heat uptake, evaporation, and the AMOC is at work under climate change<sup>49</sup>.

### Discussion

By combining observations and CMIP5/6 climate models, we identify that only models simulating a weakened AMOC can typically replicate the observed NAWH cooling and freshening. This points to the fact that the realistic AMOC has been slowing between 1900 and 2005. By constructing AMOC fingerprint indices based on dipole-like changes in SST and SSS between the subpolar gyre and near Gulf Stream regions, we find a strong and significant correlation between AMOC change and either index and demonstrate the relationship between AMOC change and the NAWH from both sides: a weakened (strengthened) AMOC corresponds to surface cooling and freshening (warming and salinifying) in the NAWH during 1900–2005. We also discovered that NAWH cooling and freshening extends beyond the surface and into the subsurface ocean. Our heat and salt budget analyses unravel that the AMOC slowdown yields a

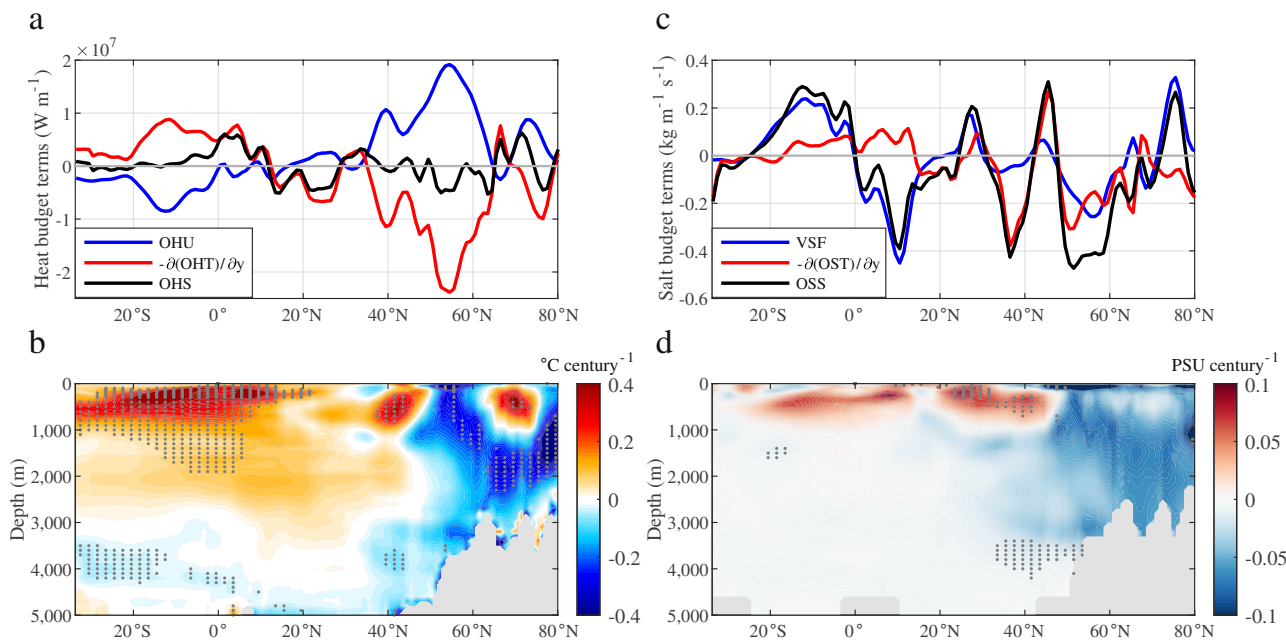


**Fig. 4 | Atlantic heat and salt budget differences between AMOC- and AMOC+.** a Difference of Atlantic heat budget (OHU, blue;  $-\partial(\text{OHT})/\partial y$ , red; OHS, black, see Methods) during 1900–2005 based on historical simulations between the MMMs of 9 AMOC- and 17 AMOC+ models (AMOC- minus AMOC+). A low-pass filter is applied with a 5-degree latitude window using the distance weighted moving average method. b Atlantic zonal-mean temperature trend difference (color shading in  $^{\circ}\text{C century}^{-1}$

century $^{-1}$ ) using the same model simulations and time period as a, c, d. Same as a, b but for differences of Atlantic salt budget and zonal-mean salinity trend between the MMMs of 2 AMOC- and 5 AMOC+ models (AMOC- minus AMOC+). The stipules refer to the regions where differences are statistically significant based on Student's t-test at 95% confidence level. Model drift from the pre-industrial control run has been removed from the model result.

meridional OHT divergence in the subpolar North Atlantic, which is partially offset by increased ocean heat uptake, leading to cooling in the full-depth water column and surface cooling over the NAWH. On the other hand, the weakened AMOC causes a meridional salt transport divergence and promotes surface freshwater input, both of which contribute to freshening in the full-depth water column and surface freshening over the NAWH. It should be noted that the relationship between AMOC weakening and NAWH SST cooling, or between AMOC strengthening and NAWH SST warming, is also visible in the CMIP anthropogenic greenhouse gas-only or aerosol-only single forcing experiment<sup>50</sup>.

We also probe the relationship between AMOC slowdown and the NAWH from different perspectives. For instance, ref. 18 showed a warming minimum to the south of Greenland in a CO<sub>2</sub> increase experiment with the slab-ocean version of ECHAM6.3 to indicate atmospheric drivers on such NAWH feature. To test the robustness of this result, we investigate the CO<sub>2</sub> warming experiments with 10 CMIP3 and CMIP5 models, in their both slab-ocean and fully coupled versions (see “Methods”). When atmospheric CO<sub>2</sub> concentrations about double, the NAWH appears along with a weakened AMOC in the MMM of fully coupled models (Fig. 5a, c), but it is absent in the MMM of slab-ocean models (Fig. 5b). The result aligns with ref. 51, suggests marked uncertainties in the formation of the NAWH in slab-ocean models, and—above all—demonstrates the contribution of a slowed AMOC to the NAWH generation.

We further elucidate AMOC effects on the NAWH using GFDL-ESM2M free- and fixed-current simulations by ref. 52 (see “Methods”). In response to increased atmospheric CO<sub>2</sub> concentrations, the AMOC decelerates from pre-industrial times in the free-current simulation (Fig. 6d) while a robust NAWH emerges to the south of Greenland (Fig. 6a). By contrast, there is no NAWH feature in the fixed-current simulation (Fig. 6b). The difference between the two illustrates SST cooling over the NAWH but warming in the vicinity of the Gulf Stream region, resembling the fingerprint of a weakened AMOC (Fig. 6c). NAWH cooling is not limited to surface but extends throughout 3000 m depth (Fig. 6e). All these

characteristics are consistent with our findings, highlighting the critical role of AMOC slowdown in the formation of the NAWH.

## Methods

### Observations

We use six monthly SST observation datasets. The Centennial in situ Observation-Based Estimates version 1 (COBESSTv1)<sup>53</sup> and version 2 (COBESSTv2)<sup>54</sup> have a horizontal resolution of 1°, with the former spanning from 1891 to 2023 and the latter from 1850 to the present. The Extended Reconstructed Sea Surface Temperature version 5 (ERSSTv5)<sup>55</sup> and version 6 (ERSSTv6)<sup>56</sup> have a horizontal resolution of 2°, with the former spanning from 1854 to the present and the latter from 1850 to the present. The Hadley Centre Sea Ice and Sea Surface Temperature (HadISST)<sup>57</sup> has a horizontal resolution of 1° from 1870 to the present. The Kaplan Extended SSTv2<sup>58</sup> has a horizontal resolution of 5° from 1856 to the present. We choose the period of 1900–2005 for SST analysis given most CMIP5 historical simulations end in 2005. All SST observations are re-gridded to 1° by 1° when calculating their average.

We also employ three monthly subsurface temperature and salinity objective analyses. The EN4 ocean temperature analysis<sup>59</sup> has a horizontal resolution of 1° with 42 vertical levels on a full-depth ocean from 1900 to the present. We take the average of the four versions with different bias corrections to represent the EN4 result. The Institute of Atmospheric Physics (IAP) ocean temperature analysis<sup>60</sup> has a horizontal resolution of 1° with 41 vertical levels from surface to 2000 m from 1940 to the present. The subsurface temperature analysis led by Ishii<sup>61</sup> has a horizontal resolution of 1° with 28 vertical levels from surface to 3000 m from 1955 to the present. We focus on the period of 1955–2005 when data from all three analyses are available and use the top-layer (EN4: 5 m, IAP: 1 m, Ishii: 0 m) salinity to represent SSS.

### Climate model simulations

We leverage pre-industrial control (piControl) and ensemble-historical simulations of 41 CMIP5 models and 53 CMIP6 models (Supplementary

**Fig. 5 | Atlantic SST and AMOC changes in slab-ocean and fully coupled model experiments.**

**a, b** Atlantic surface temperature changes (color shading in °C) as atmospheric CO<sub>2</sub> concentrations about double for the MMMs of **a** slab-ocean and **b** fully coupled versions of 10 CMIP3/5 models (see “Methods”). **c** Timeseries of AMOC strength in the 1pcto2x/1pctco2 experiments for the MMM of 10 fully coupled CMIP3/5 models. The linear regression line (gray dashed) denotes the AMOC decline trend.

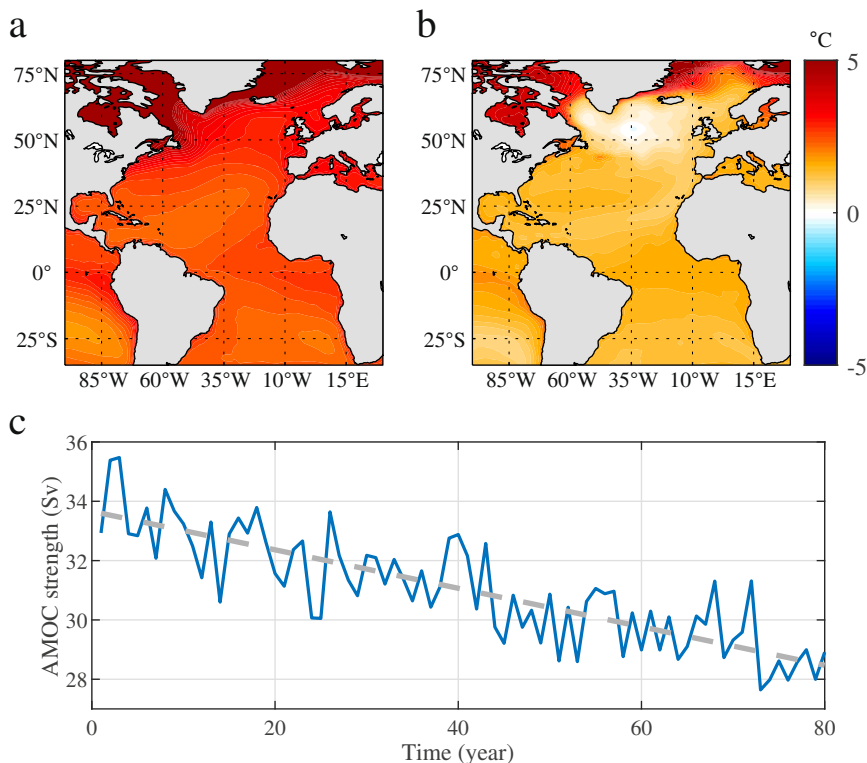


Table 1) in which the AMOC strength is derived from the maximum of the meridional overturning stream function below 500 m in the North Atlantic. When calculating the temperature, salinity, and AMOC trends, we average over ensembles for each model, and average over models for multi-model mean (MMM). The trends from piControl are removed to prevent model drift. To analyze oceanic heat budget, we use piControl and ensemble-historical simulations of 5 CMIP5 models and 21 CMIP6 models (Supplementary Table 1), which include variables for calculating all budget terms. For each model, we calculate its ensemble mean and remove its piControl value. Similarly, we use piControl and ensemble-historical simulations of 7 CMIP6 models (Supplementary Table 1) for Atlantic salt budget analysis. To align with observations and to be consistent to the greatest extent, we choose the period of 1900–2005 for SST, SSS, subsurface temperature and salinity, and heat and salt budget analyses for CMIP5/6 historical simulations.

We notice large inter-model difference in deep convection/mixing in the North Atlantic among either CMIP5<sup>16,62,63</sup> or CMIP6 models<sup>64</sup>, as well as discrepancy from observation, or namely, model bias<sup>62–64</sup>. However, while deep mixing region and NAWH site may differ amongst models, the former is usually downstream of the latter<sup>16</sup>. Thereupon, the different NAWH locations across models or between model and observation could potentially relate to inter-model difference or model bias in deep convection/mixing in the North Atlantic. We also notice large inter-model difference in AMOC change. The inter-model spread on AMOC and NAWH simulations could affect anthropogenic carbon uptake in the North Atlantic<sup>65</sup>, and the inter-hemispheric asymmetry of temperature and precipitation<sup>66</sup>.

Also, we adopt Geophysical Fluid Dynamics Laboratory Earth System Model 2 (GFDL ESM2M) free- and fixed-current simulations from ref. 52. They are two 100-year simulations forced with a transient increase of 1% atmospheric CO<sub>2</sub> per year (1pcto2x) from piControl. One is a free-running forced experiment (free-current) with a changing AMOC, while the other while the other is a fixed-circulation experiment (fixed-current) in which ocean currents are programmed to follow a fixed seasonal cycle in GFDL ESM2M piControl<sup>67</sup>.

Additionally, we employ slab-ocean and fully coupled versions with ten climate models. They are 8 CMIP3 models (cccma\_cgcm3\_1, csiro\_mk3\_0,

giss\_model\_e\_r, miroc3\_2\_hires, miroc3\_2\_medres, mpi\_echam5, mri\_cgcm2\_3\_2a and ukmo\_hadgem1)<sup>68</sup> and 2 CMIP5 models (CCSM4 and CESM1-CAM5, both having ~1-degree resolution in all components)<sup>21</sup>. For CMIP3/5 slab-ocean models, we use their pre-industrial or present-day control runs, and abruptly doubled CO<sub>2</sub> (2xco2) experiments based on their control runs. We compare the last 10 years average of the 2xco2 experiment to the last 10 years average in the corresponding control runs. For CMIP3 fully coupled models, we resort to their 1% per year CO<sub>2</sub> increase to doubling (1pcto2x) experiments. We perform 1pctco2 experiments on CMIP5 fully coupled models based on their piControl runs. We compare the difference between the average of years 71–80 and the average of years 1–10 in 1pcto2x for CMIP3 models and in 1pctco2 for CMIP5 models.

#### AMOC fingerprint index

We develop the AMOC fingerprint index (FPI) based on the dipole pattern of SST or SSS trend from CMIP5/6 models. Although the locations of the dipoles may vary among models, for consistency, we define the subpolar gyre region as 46–58°N, 49–21°W, and the near Gulf Stream region as 41–45°N, 66–40°W according to the CMIP5/6 MMM. For all the models, we calculate SST<sub>SG</sub> and SSS<sub>SG</sub> as the area-averaged SST and SSS anomalies in the subpolar gyre region, SST<sub>GS</sub> and SSS<sub>GS</sub> as the area-averaged SST and SSS anomalies in the near Gulf Stream region in historical simulations with respect to their piControl values. The SST- and SSS-based AMOC fingerprint indices (FPI<sub>SST</sub> and FPI<sub>SSS</sub>) are defined as

$$FPI_{SST} = SST_{SG} - SST_{GS} \quad (1)$$

$$FPI_{SSS} = SSS_{SG} - SSS_{GS} \quad (2)$$

Also, we compare our FPI<sub>SST</sub> with I<sub>AMOC</sub> defined by ref. 17, that is,

$$I_{AMOC} = SST_{sg} - SST_{global} \quad (3)$$

where SST<sub>sg</sub> denotes the mean SST of the subpolar gyre region defined by ref. 17, and SST<sub>global</sub> denotes globally averaged SST. To align with our FPI<sub>SST</sub> calculation and eliminate the effect of time window selection, we utilize

annual mean SST rather than winter and spring months (November to May) SST in the calculation of  $I_{AMOC}$ . We find that the correlation between AMOC and  $I_{AMOC}$  trends ( $0.53, p < 0.01$ ) over 1900–2005 is nearly as strong and significant as our FPI<sub>SST</sub> result ( $0.57, p < 0.01$ ), which demonstrates the robustness of our AMOC fingerprint index (Supplementary Fig. 6).

### Oceanic heat and salt budget analysis

We conduct an ocean heat budget analysis in the Atlantic basin with components of ocean heat uptake, transport, and storage<sup>2,50,69</sup>. At a certain latitude, the full-depth integrated ocean heat content (OHC) is

$$OHC = \int_{x_w}^{x_e} \int_{-H}^0 \rho_0 C_p \theta dz dx \quad (4)$$

where  $x_w$  and  $x_e$  denote the longitudes of the western and eastern boundaries of the Atlantic basin at that latitude,  $\rho_0$  is sea water density,  $C_p$  is the specific heat of sea water,  $\theta$  is potential temperature of sea water, and  $-H$  denotes the depth of ocean bottom. Ocean heat storage (OHS) is defined as OHC tendency, that is,

$$OHS = \frac{\partial}{\partial t} OHC = \frac{\partial}{\partial t} \int_{x_w}^{x_e} \int_{-H}^0 \rho_0 C_p \theta dz dx \quad (5)$$

The integrated ocean heat uptake (OHU) is

$$OHU = \int_{x_w}^{x_e} (SHF) dx \quad (6)$$

where SHF denotes the net downward surface heat flux. The meridional OHT is

$$OHT = \int_{x_w}^{x_e} \int_{-H}^0 \rho_0 C_p (v\theta + D_T) dz dx \quad (7)$$

where  $v$  is three-dimensional velocity and  $D_T$  represents diffusion processes of heat. The heat budget is then written as

$$OHS = OHU - \frac{\partial}{\partial y} OHT \quad (8)$$

which means that OHS is determined by heat uptake from atmosphere and heat redistribution in form of the meridional gradient of OHT.

Likewise, we conduct Atlantic salt budget analysis with components of virtual salt flux (VSF), ocean salt transport (OST), and ocean salt storage, where surface freshwater flux ( $F_W$ ) is converted into an equivalent virtual salt flux ( $F_V$ ), that is,

$$F_V = -F_W SSS \quad (9)$$

where SSS denotes sea surface salinity<sup>70</sup>. The salt budget can be written as

$$OSS = VSF - \frac{\partial}{\partial y} OST \quad (10)$$

where OSS denotes ocean salt storage, and the integrated net downward surface virtual salt flux is

$$VSF = \int_{x_w}^{x_e} (F_V) dx \quad (11)$$

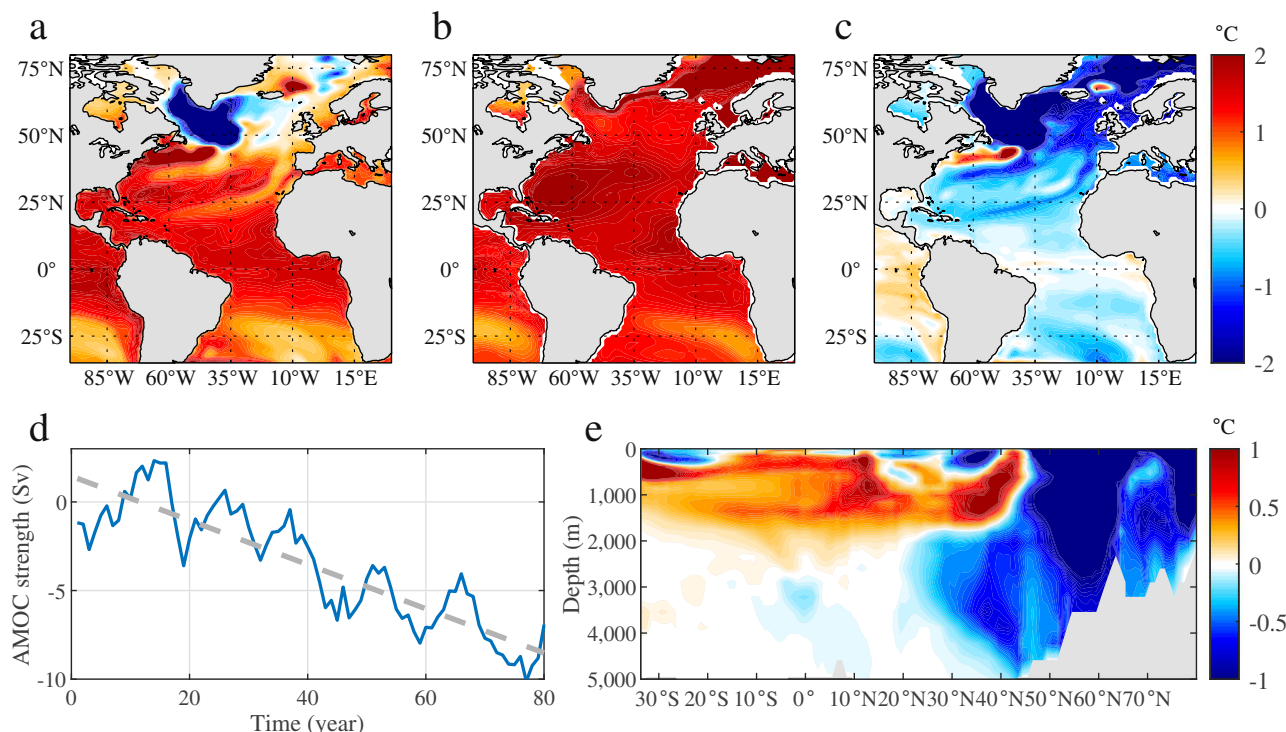


**Fig. 6 | Atlantic SST and zonal-mean ocean temperature changes in GFDL-ESM2M free- and fixed-current simulations.** **a–c** Atlantic SST changes (color shading in °C) in GFDL-ESM2M (a) free- and (b) fixed-current 1pctco2 experiment over years 71–80 relative to the pre-industrial control run, and (c) the difference between the two (a minus b). **d** Timeseries of AMOC strength

anomaly in GFDL-ESM2M 1pctco2 experiment relative to the pre-industrial control run. The linear regression line (gray dashed) denotes the AMOC decline trend. **e** Atlantic zonal-mean temperature difference (color shading in °C) between GFDL-ESM2M free- and fixed-current 1pctco2 experiment over years 71–80 (free minus fixed).

The meridional salt transport is

$$OST = \int_{x_w}^{x_e} \int_{-H}^0 \rho_0 (vs + D_S) dz dx \quad (12)$$

where  $s$  is salinity of sea water and  $D_S$  represents diffusion processes of salt. According to the budget, OSS is determined by surface virtual salt flux and salt redistribution in form of the meridional gradient of OST.

### Statistical significance test

We use the Student's t-test to determine the statistical significance of the linear trend and calculate the p-value to see if it deviates significantly from a zero trend. We use the Student's t-test to compare AMOC- and AMOC+ at the 95% confidence level. We also use the Pearson correlation significance test with a degree of freedom of  $n$ , where  $n$  represents the number of models.

### Data availability

COBESST v1 data are available at <https://psl.noaa.gov/data/gridded/data.cobe.html>. COBESST v2 data are available at <https://psl.noaa.gov/data/gridded/data.cobe2.html>. ERSST v5 data are available at <https://www.ncei.noaa.gov/products/extended-reconstructed-sst>. ERSST v6 data are available at <https://www.ncei.noaa.gov/pub/data/cmb/ersst/v5/2023.ersst.v6/>. HadISST data are available at <https://www.metoffice.gov.uk/hadobs/hadisst/>. Kaplan Extended SST v2 data are available at [https://psl.noaa.gov/data/gridded/data.kaplan\\_sst.html](https://psl.noaa.gov/data/gridded/data.kaplan_sst.html). EN4 data are available at <https://www.metoffice.gov.uk/hadobs/en4/download-en4-2-2.html>. IAP data are available at <http://www.ocean.iap.ac.cn/pages/dataService/dataService.html?navAnchor=dataService>. Ishii data are available at <https://climate.mri-jma.go.jp/pub/ocean/ts/v7.3.1/>. CMIP3 model data are available at <https://aims2.llnl.gov/search/cmip3/>. CMIP5 model data are available at <https://aims2.llnl.gov/search/cmip5/>. CMIP6 model data are available at <https://aims2.llnl.gov/search/cmip6/>. GFDL-ESM2M 1pctCO<sub>2</sub> free- and fixed-current experiments data are available at <https://doi.org/10.1594/PANGAEA.914424>.

### Code availability

The source codes of CCSM4 and CESM1 are available at <https://www.cesm.ucar.edu/models/releases>. The mapping package for MATLAB is from Pawlowicz, R. (2020) "M\_Map: A mapping package for MATLAB", version 1.4 m, [Computer software], and available at [www.eoas.ubc.ca/~rich/map.html](http://www.eoas.ubc.ca/~rich/map.html).

Received: 17 January 2025; Accepted: 19 May 2025;

Published online: 28 May 2025

### References

- Zhang, R. et al. A review of the role of the Atlantic meridional overturning circulation in Atlantic multidecadal variability and associated climate impacts. *Rev. Geophys.* **57**, 316–375 (2019).
- Liu, W., Fedorov, A. V., Xie, S.-P. & Hu, S. Climate impacts of a weakened Atlantic meridional overturning circulation in a warming climate. *Sci. Adv.* **6**, eaaz4876 (2020).
- Hu, A. et al. 2020. Role of AMOC in transient climate response to greenhouse gas forcing in two coupled models. *J. Clim.* **33**, 5845–5859 (2020).
- Kilbourne, K. H. et al. Atlantic circulation change still uncertain. *Nat. Geosci.* **15**, 165–167 (2022).
- Rahmstorf, S. et al. Exceptional twentieth-century slowdown in Atlantic Ocean overturning circulation. *Nat. Clim. Change* **5**, 475 (2015).
- Thornalley, D. J. R. et al. Anomalously weak Labrador Sea convection and Atlantic overturning during the past 150 years. *Nature* **556**, 227–230 (2018).
- Caesar, L., McCarthy, G. D., Thornalley, D. J. R., Cahill, N. & Rahmstorf, S. Current Atlantic meridional overturning circulation weakest in last millennium. *Nat. Geosci.* **14**, 118–120 (2021).
- IPCC. *Climate Change 2013: The Physical Science Basis*. Contribution of Working Group I to the Fifth Assessment Report of the Intergovernmental Panel on Climate Change (eds Stocker, T. F. et al.) (Cambridge Univ. Press, 2013).
- IPCC. *Climate Change 2021: The Physical Science Basis*. Contribution of Working Group I to the Sixth Assessment Report of the Intergovernmental Panel on Climate Change (eds Masson-Delmotte, V. et al.) (Cambridge Univ. Press, 2021).
- Hansen, J., Ruedy, R., Sato, M. & Lo, K. Global surface temperature change. *Rev. Geophys.* **48**, RG4004 (2010).
- Liu, W. et al. Extended reconstructed sea surface temperature version 4 (ERSST.v4): part II. Parametric and structural uncertainty estimations. *J. Clim.* **28**, 931–951 (2015).
- Drijfhout, S., Van Oldenborgh, G. J. & Cimatoribus, A. Is a decline of AMOC causing the warming hole above the North Atlantic in observed and modeled warming patterns?. *J. Clim.* **25**, 8373–8379 (2012).
- Russell, G. L. & Rind, D. Response to CO<sub>2</sub> transient increase in the GISS coupled model: regional coolings in a warming climate. *J. Clim.* **12**, 531–539 (1999).
- Kim, H. & An, S.-I. On the subarctic North Atlantic cooling due to global warming. *Theor. Appl. Climatol.* **114**, 9–19 (2013).
- Gervais, M., Shaman, J. & Kushnir, Y. Mechanisms governing the development of the North Atlantic warming hole in the CESM-LE future climate simulations. *J. Clim.* **31**, 5927–5946 (2018).
- Menary, M. B. & Wood, R. A. An anatomy of the projected North Atlantic warming hole in CMIP5 models. *Clim. Dyn.* **50**, 3063–3080 (2018).
- Caesar, L., Rahmstorf, S., Robinson, A., Feulner, G. & Saba, V. Observed fingerprint of a weakening Atlantic Ocean overturning circulation. *Nature* **556**, 191–196 (2018).
- Keil, P. et al. Multiple drivers of the North Atlantic warming hole. *Nat. Clim. Change* **10**, 667–671 (2020).
- Li, L., Lozier, M. S. & Li, F. Century-long cooling trend in subpolar North Atlantic forced by atmosphere: an alternative explanation. *Clim. Dyn.* **58**, 2249–2267 (2022).
- Hu, S. & Fedorov, A. V. Indian Ocean warming as a driver of the North Atlantic warming hole. *Nat. Commun.* **11**, 4785 (2020).
- He, C. et al. A North Atlantic warming hole without ocean circulation. *Geophys. Res. Lett.* **49**, e2022GL100420 (2022).
- Fan, Y., Liu, W., Zhang, P., Chen, R. & Li, L. North Atlantic Oscillation contributes to the subpolar North Atlantic cooling in the past century. *Clim. Dyn.* **61**, 5199–5215 (2023).
- Timmermann, A. & Goosse, H. Is the wind stress forcing essential for the meridional overturning circulation?. *Geophys. Res. Lett.* **31**, L04303 (2004).
- Bryden, H. L. Wind-driven and buoyancy-driven circulation in the subtropical North Atlantic Ocean. *Proc. Math. Phys. Eng. Sci.* **477**, 20210172 (2021).
- Mimi, M. S. & Liu, W. Atlantic meridional overturning circulation slowdown modulates wind-driven circulations in a warmer climate. *Commun. Earth Environ.* **5**, 727 (2024).
- Timmermann, A., Latif, M., Voss, R. & Grotzner, A. Northern hemispheric interdecadal variability: a coupled air-sea mode. *J. Clim.* **11**, 1906–1930 (1998).
- Wen, N., Frankignoul, C. & Gastineau, G. Active AMOC-NAO coupling in the IPSL-CM5A-MR climate model. *Clim. Dyn.* **47**, 2105–2119 (2016).
- Ma, X. et al. Evolving AMOC multidecadal variability under different CO<sub>2</sub> forcings. *Clim. Dyn.* **57**, 593–610 (2021).
- Johns, W. E. et al. Continuous, array-based estimates of Atlantic Ocean heat transport at 26.5°. *N. J. Clim.* **24**, 2429–2449 (2011).

30. McDonagh, E. L. et al. Continuous estimate of Atlantic oceanic freshwater flux at 26.5° N. *N. J. Clim.* **28**, 8888–8906 (2015).

31. Johns, W. E. et al. Towards two decades of Atlantic Ocean mass and heat transports at 26.5° N. *Philos. Trans. A Math. Phys. Eng. Sci.* **381**, 20220188 (2023).

32. Bryden, H. L. et al. Reduction in ocean heat transport at 26°N since 2008 cools the eastern subpolar gyre of the North Atlantic Ocean. *J. Clim.* **33**, 1677–1689 (2020).

33. Smeed, D. A. et al. The North Atlantic Ocean is in a state of reduced overturning. *Geophys. Res. Lett.* **45**, 1527–1533 (2018).

34. Roberts, C. D., Jackson, L. & McNeall, D. Is the 2004–2012 reduction of the Atlantic meridional overturning circulation significant? *Geophys. Res. Lett.* **41**, 3204–3210 (2014).

35. Weaver, A. J. et al. Stability of the Atlantic meridional overturning circulation: a model intercomparison. *Geophys. Res. Lett.* **39**, L20709 (2012).

36. Jackson, L. C. et al. The evolution of the North Atlantic meridional overturning circulation since 1980. *Nat. Rev. Earth Environ.* **3**, 241–254 (2022).

37. Menary, M. B. et al. Aerosol-forced AMOC changes in CMIP6 historical simulations. *Geophys. Res. Lett.* **47**, e2020GL088166 (2020).

38. Hassan, T., Allen, R. J., Liu, W. & Randles, C. A. Anthropogenic aerosol forcing of the Atlantic meridional overturning circulation and the associated mechanisms in CMIP6 models. *Atmos. Chem. Phys.* **21**, 5821–5846 (2021).

39. McCarthy, G. D. & Caesar, L. Can we trust projections of AMOC weakening based on climate models that cannot reproduce the past? *Philos. Trans. R. Soc. A* **381**, 20220193 (2023).

40. Fan, Y., Chan, D., Zhang, P. & Li, L. Disagreement on the North Atlantic cold blob formation mechanisms among climate models. *J. Clim.* **37**, 4061–4078 (2024).

41. Holliday, N. P. et al. Ocean circulation causes the largest freshening event for 120 years in eastern subpolar North Atlantic. *Nat. Commun.* **11**, 585 (2020).

42. Oltmanns, M., Karstensen, J., Moore, G. W. K. & Josey, S. A. Rapid cooling and increased storminess triggered by freshwater in the North Atlantic. *Geophys. Res. Lett.* **47**, e2020GL087207 (2020).

43. Zhu, C. & Liu, Z. Weakening Atlantic overturning circulation causes South Atlantic salinity pile-up. *Nat. Clim. Change* **10**, 998–1003 (2020).

44. Hausmann, U., Czaja, A. & Marshall, J. Mechanisms controlling the SST air-sea heat flux feedback and its dependence on spatial scale. *Clim. Dyn.* **48**, 1297–1307 (2017).

45. Zhang, L. & Cooke, W. Simulated changes of the Southern Ocean air-sea heat flux feedback in a warmer climate. *Clim. Dyn.* **56**, 1–16 (2021).

46. Stommel, H. Thermohaline convection with two stable regimes of flow. *Tellus* **13**, 224–230 (1961).

47. Liu, W., Liu, Z. & Brady, E. C. Why is the AMOC monostable in coupled general circulation models? *J. Clim.* **27**, 2427–2443 (2014).

48. Liu, W., Xie, S. P., Liu, Z. & Zhu, J. Overlooked possibility of a collapsed Atlantic meridional overturning circulation in warming climate. *Sci. Adv.* **3**, e1601666 (2017).

49. Ma, X., Liu, W., Allen, R., Huang, G. & Li, X. Dependence of regional ocean heat uptake on anthropogenic warming scenarios. *Sci. Adv.* **6**, eabc0303 (2020).

50. Li, S., Liu, W., Allen, R. J., Shi, J.-R. & Li, L. Ocean heat uptake and interbasin redistribution driven by anthropogenic aerosols and greenhouse gases. *Nat. Geosci.* **16**, 695–703 (2023).

51. Woollings, T., Gregory, J. M., Pinto, J. G., Reyers, M. & Brayshaw, D. J. Response of the North Atlantic storm track to climate change shaped by ocean-atmosphere coupling. *Nat. Geosci.* **5**, 313–317 (2012).

52. Winton, M., Griffies, S. M., Samuels, B. L., Sarmiento, J. L. & Frölicher, T. L. Connecting changing ocean circulation with changing climate. *J. Clim.* **26**, 2268–2278 (2013).

53. Ishii, M., Shouji, A., Sugimoto, S. & Matsumoto, T. Objective analyses of sea-surface temperature and marine meteorological variables for the 20th century using ICOADS and the Kobe collection. *Int. J. Climatol.* **25**, 865–879 (2005).

54. Hihara, S., Ishii, M. & Fukuda, Y. Centennial-scale sea surface temperature analysis and its uncertainty. *J. Clim.* **27**, 57–75 (2014).

55. Huang, B., Liu, C., Ren, G., Zhang, H.-M. & Zhang, L. The role of buoy and Argo observations in two SST analyses in the global and tropical Pacific oceans. *J. Clim.* **32**, 2517–2535 (2018).

56. Huang, B. et al. Extended reconstructed sea surface temperature, version 6 (ERSSTv6). part I: an artificial neural network approach. *J. Clim.* **38**, 1105–1121 (2025).

57. Rayner, N. A. et al. Global analyses of sea surface temperature, sea ice, and night marine air temperature since the late nineteenth century. *J. Geophys. Res.* **108**, 4407 (2003).

58. Kaplan, A. et al. Analyses of global sea surface temperature 1856–1991. *J. Geophys. Res.* **103**, 18567–18589 (1998).

59. Good, S. A., Martin, M. J. & Rayner, N. A. EN4: quality controlled ocean temperature and salinity profiles and monthly objective analyses with uncertainty estimates. *J. Geophys. Res. Oceans* **118**, 6704–6716 (2013).

60. Cheng, L. et al. Improved estimates of ocean heat content from 1960 to 2015. *Sci. Adv.* **3**, e1601545 (2017).

61. Ishii, M., Shouji, A., Sugimoto, S. & Matsumoto, T. Objective analyses of SST and marine meteorological variables for the 20th century using COADS and the Kobe Collection. *Int. J. Climatol.* **25**, 865–879 (2005).

62. Heuzé, C. North Atlantic deep water formation and AMOC in CMIP5 models. *Ocean Sci.* **13**, 609–622 (2017).

63. Liu, W., Fedorov, A. & Sévellec, F. The mechanisms of the Atlantic meridional overturning circulation slowdown induced by Arctic Sea ice decline. *J. Clim.* **32**, 977–996 (2019).

64. Heuzé, C. Antarctic bottom water and North Atlantic deep water in CMIP6 models. *Ocean Sci.* **17**, 59–90 (2021).

65. Park, I.-H. et al. Present-day North Atlantic salinity constrains future warming of the Northern Hemisphere. *Nat. Clim. Chang.* **13**, 816–822 (2023).

66. Park, I.-H. et al. North Atlantic warming hole modulates interhemispheric asymmetry of future temperature and precipitation. *Earth's Future* **12**, e2023EF004146 (2024).

67. Bronselaer, B. & Zanna, L. Heat and carbon coupling reveals ocean warming due to circulation changes. *Nature* **584**, 227–233 (2020).

68. Randall, D. A. et al. in *IPCC Climate Change 2007: The Physical Science Basis* (eds Solomon, S. et al) Ch. 8 (Cambridge Univ. Press, 2007).

69. Liu, W., Lu, J., Xie, S.-P. & Fedorov, A. Southern Ocean heat uptake, redistribution, and storage in a warming climate: the role of meridional overturning circulation. *J. Clim.* **31**, 4727–4743 (2018).

70. Yin, J., Stouffer, R. J., Spelman, M. J. & Griffies, S. M. Evaluating the uncertainty induced by the virtual salt flux assumption in climate simulations and future projections. *J. Clim.* **23**, 80–96 (2010).

## Acknowledgements

This study has been supported by U.S. National Science Foundation (OCE-2123422, AGS-2053121, and AGS-2237743).

## Author contributions

K.-Y.L. performed the analysis and wrote the original draft of the paper. W.L. conceived the study. Both authors contributed to interpreting the results and made improvements to the paper.

## Competing interests

The authors declare no competing interests.

## Additional information

**Supplementary information** The online version contains supplementary material available at <https://doi.org/10.1038/s43247-025-02403-0>.

**Correspondence** and requests for materials should be addressed to Wei Liu.

**Peer review information** *Communications Earth & Environment* thanks the anonymous reviewers for their contribution to the peer review of this work. Primary Handling Editors: Sreelekha Jarugula and Alice Drinkwater. A peer review file is available.

**Reprints and permissions information** is available at <http://www.nature.com/reprints>

**Publisher's note** Springer Nature remains neutral with regard to jurisdictional claims in published maps and institutional affiliations.

**Open Access** This article is licensed under a Creative Commons Attribution 4.0 International License, which permits use, sharing, adaptation, distribution and reproduction in any medium or format, as long as you give appropriate credit to the original author(s) and the source, provide a link to the Creative Commons licence, and indicate if changes were made. The images or other third party material in this article are included in the article's Creative Commons licence, unless indicated otherwise in a credit line to the material. If material is not included in the article's Creative Commons licence and your intended use is not permitted by statutory regulation or exceeds the permitted use, you will need to obtain permission directly from the copyright holder. To view a copy of this licence, visit <http://creativecommons.org/licenses/by/4.0/>.

© The Author(s) 2025